Journal of Materials Chemistry A

ROYAL SOCIETY OF CHEMISTRY

COMMUNICATION

View Article Online
View Journal | View Issue

Cite this: *J. Mater. Chem. A*, 2021, **9**, 4687

Received 5th January 2021
Accepted 1st February 2021

DOI: 10.1039/d1ta00100k

rsc.li/materials-a

Integrating active C_3N_4 moieties in hydrogen-bonded organic frameworks for efficient photocatalysis†

Tao Li,[ab] Bai-Tong Liu,[b] Zhi-Bin Fang,[b] Qi Yin,[b] Rui Wang[b] and Tian-Fu Liu *[ab]

Hydrogen-bonded organic frameworks (HOFs) provide a platform to self-assemble numerous functional species into an ordered structure. Herein, a well-known photoactive C_3N_4 moiety was integrated into an HOF structure (PFC-42) with the merits of high porosity and crystallinity. Under visible-light irradiation, the Pt nanoparticle-loaded PFC-42 (PFC-42-Pt) continuously produces hydrogen from water in the presence of scavengers with the evolution rate of 11.32 mmol g^{-1}, which is outstanding among all the reported Pt/porous composite materials. The significantly high H_2 evolution of PFC-42-Pt compared with that of amorphous analogue bulk C_3N_4–Pt and nanosheet C_3N_4–Pt demonstrates that the ordered arrangement of photosensitizers dramatically improves the photocatalytic activity of the material, which is further proved by the recrystallization experiment. This study represents the first example of HOF capable of photocatalysis, not only demonstrating the great application potentials of HOF in heterogeneous photocatalysis but also rendering an excellent opportunity to reveal structure–activity relations.

Introduction

Photocatalytic water splitting has been regarded as a feasible strategy for the effective use of solar energy to solve increasingly serious environmental and energy problems.[1–3] Although most reported photocatalysts for water splitting are based on inorganic semiconductors,[4–6] organic semiconductors such as polymeric carbon nitride, poly(azomethine)s,[7] conjugated microporous polymers (CMPs),[8,9] and linear conjugated polymers[10] have also demonstrated their promising potentials for photocatalysis with the merits of abundant reserves and low cost.[11] However, these materials are usually nonporous, which limits the transmission of active species across the catalyst surface. Moreover, it is hard to know the structure–activity relationship due to the lack of precise structural information, and the amorphous form always brings in difficulties on precise structure control and modification.[12] Therefore, it is not hard to imagine that the self-assembly of photoactive ligands into a porous and ordered structure would promote the activity of the catalytic species.

HOFs, as a class of porous crystalline materials self-assembled by organic ligands through hydrogen bonds, have drawn significant interest for a wide range of applications such as in gas separation[13,14] and storage,[15,16] sensing,[17–19] biomedicine,[20,21] and photoluminescence.[22,23] Despite their versatility, the application of HOFs in the field of photocatalysis is still very rare. If one can integrate photoactive species into HOFs, the ordered structure combined with the tunable pore size and large surface area should greatly benefit the photocatalytic performance. Moreover, the explicit structural information could help in the establishment of structure–performance relationships and provide insights into the photocatalytic mechanism. In particular, exogenous catalytic species can be stabilized inside the pores of HOFs *via* one-pot synthesis or post-synthetic modification. Given these considerations, we are encouraged to exploit HOF materials as photocatalysts.

In this study, we have successfully designed and synthesized an organic linker comprising the well-known organic photoactive carbon nitride unit (heptazine, abbreviated as C_3N_4). The self-assembly of this ligand gave rise to a two-dimensional layered HOF named as PFC-42 (PFC = porous materials from FJIRSM, CAS). The post functionalization of HOF afforded a Pt nanoparticle well-dispersed HOF composite denoted as PFC-42-Pt. The photocatalytic reaction revealed that PFC-42-Pt exhibited an excellent H_2 production rate of 11.32 mmol g^{-1} under visible-light illumination (λ > 400 nm). The bulk PFC-42-Pt photocatalytic activity is much higher than that of bulk C_3N_4–Pt, which is 3.5 times higher than that of nanosheet C_3N_4–Pt.

[a]*College of Chemistry and Materials Science, Fujian Normal University, Fuzhou 350002, P. R. China. E-mail: tfliu@fjirsm.ac.cn*

[b]*State Key Laboratory of Structural Chemistry, Fujian Institute of Research on the Structure of Matter, Chinese Academy of Sciences, Fuzhou 350002, P. R. China*

† Electronic supplementary information (ESI) available. CCDC 2035078. For ESI and crystallographic data in CIF or other electronic format see DOI: 10.1039/d1ta00100k

Single-crystal (Fig. S1†) X-ray diffraction reveals that PFC-42 crystallizes in the trigonal space group $P2_1/n$ (Table S1†). PFC-42 exhibits a distinctive two-dimensional (2D) framework. Each H_3HTB molecule interacts with two neighboring ones through two O–H···O hydrogen bonds, extending into a one-dimensional layer (Fig. 1a). The O–H···O distance is 2.52 Å, falling into the hydrogen bond range according to literature (2.49 Å to 3.15 Å). These chains expand to a 2D square layer (sql) *via* van der Waals interactions. Adjacent 2D square layers (sql) stack in the ABAB mode *via* intermolecular π–π interactions (Fig. 1b), leaving one-dimensional channels of 5.52 Å × 8.63 Å along the *c*-axis (Fig. S2†). The PLATON analysis indicates that the simulated solvent-accessible void space is 765.2 $Å^3$, which accounts for 26.5% of the entire unit cell volume. The experimental PXRD pattern of PFC-42 is consistent with the corresponding theoretical pattern deduced from single-crystal X-ray data, indicating the phase purity of the bulk PFC-42 (Fig. S3†). Thermogravimetric analysis indicated that PFC-42 did not show obvious weight loss until 395 K (Fig. S4†). PXRD patterns of PFC-42 after being immersed in methanol and water, respectively, match well with that of the as-synthesized one (Fig. S5†). All the above-mentioned results manifest that PFC-42 possesses good thermal, water, and chemical stability.

As revealed by the UV/Vis absorption curve (Fig. S6†) and Kubelka–Munk plot, the absorption edge of PFC-42 is 539 nm with a bandgap of 2.30 eV. As an efficient photocatalyst, the material needs to have not only an appropriate bandgap, but also matched conduction band (CV) and valence band (VB) relative to the redox potential of the photocatalytic reaction. The conduction-band position was estimated *via* the Mott–Schottky plot (Fig. 2a). The positive slope indicates a typical n-type semiconductor characteristic for PFC-42. The CB of PFC-42 was estimated to be ≈ −0.51 V (*vs.* normal hydrogen electrode (NHE)), and the VB of the material was calculated to be ≈1.79 V (NHE) based on the bandgap obtained from the Kubelka–Munk plot. These results manifest that the band alignment of PFC-42 meets the thermodynamic demands for the reduction half-reactions of water spitting.

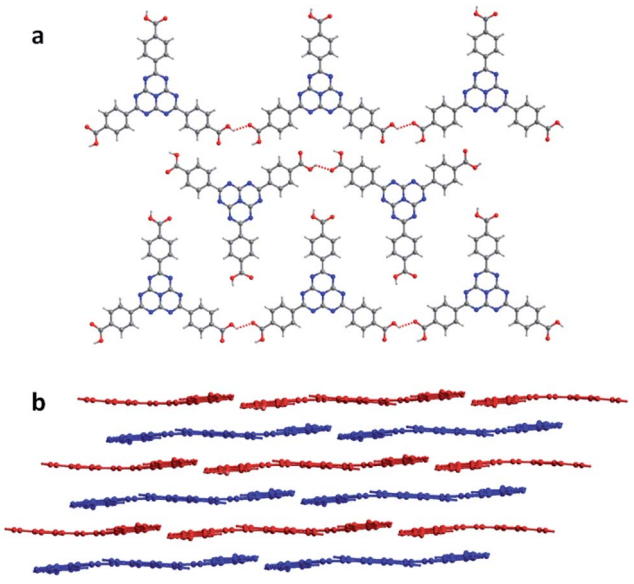

Fig. 1 (a) Crystal structure of PFC-42 composed of heptazine-based building blocks. Color codes: blue N, red O, grey C. (b) ABAB packing mode of PFC-42 viewed along the *b*-axis.

Although bare PFC-42 powder is little active for water splitting, the activity is very low, as observed by other pure g-C_3N_4 systems. To solve this problem, Pt was introduced into PFC-42 as a cocatalyst *via* the post-synthetic metalation as usually done in other photocatalysis reactions. The high magnification transmission electron microscopy (TEM) image of PFC-42-Pt indicates Pt nanoparticles (PtNPs) with a diameter of about 3 to 5 nm were evenly embedded in the porous PFC-42 (Fig. 3a and b). Pt 4f core-level XPS spectra show that Pt(II) (Pt $4f_{7/2}$ peak at 72.5 eV) and Pt(0) species (Pt $4f_{7/2}$ peak at 70.9 eV) coexisted in the catalyst, which was probably caused by the incomplete reduction of the Pt precursor or partial oxidation when exposing the sample in the air (Fig. 3d).[24,25] Moreover, the binding energy of N 1s (from heptazine) shifted from 401.6 eV to 401.9 eV in XPS spectra after Pt loading (Fig. S8†).[26] These results suggest that the PtNP in the framework probably attached to the heptazine nitrogen atoms and caused a decrease in the electron density of N atoms. PXRD of PFC-42-Pt did not show any peak from Pt particles due to the small grain size, low content, and even distribution of Pt particles (Fig. S9†).

The hydrogen evolution activities of PFC-42-Pt were evaluated under visible-light irradiation in the presence of electron scavengers. The H_2 production rates varied with the Pt loading amount in PFC-42 (Fig. 2b). Among which, 1.54% Pt loading gave rise to the highest rate of 11.32 mmol g^{-1} in 5 h. FT-IR (Fig. 2c), PXRD (Fig. S9†), and XPS analyses (Fig. S12†) before and after the catalytic reaction indicate that PFC-42 is a durable photocatalyst for H_2 evolution.

In order to manifest the merit of the ordered arrangement of photosensitizers for photocatalytic activity, we also synthesized the amorphous analogue of PFC-42, bulk C_3N_4 (Fig. S13†), and nanosheet C_3N_4 (Fig. S14†) for comparison, followed by the photocatalysis investigation. After the same Pt loading procedure as conducted on PFC-42, the Pt-modified bulk C_3N_4 (named as bulk C_3N_4–Pt) barely showed any activity towards H_2 evolution under the same reaction conditions. Nano-sheet C_3N_4 with PtNP loading (sheet C_3N_4–Pt) shows activity towards H_2 production, which is much lower than PFC-42-Pt (Fig. 3c). These results indicate that the ordered arrangement of the photosensitizer combined with a large accessible surface greatly boosts the photocatalytic activity of the material. This can also be confirmed by the phenomena that detracting the crystallinity and porosity of PFC-42-Pt *via* the acid treatment would dramatically decrease its catalytic activity (Fig. S15†). The crystallinity of the acid-damaged PFC-42-Pt can be repaired by simply recrystallizing in methanol, and the photocatalytic activity was recovered to 85.6% of its original rate (Fig. S16†). Therefore, we demonstrated that the ordered arrangement of photosensitizers greatly boosts the photocatalytic activity and indicates the unique advantage of easy recovery and recyclability of HOF catalysts.

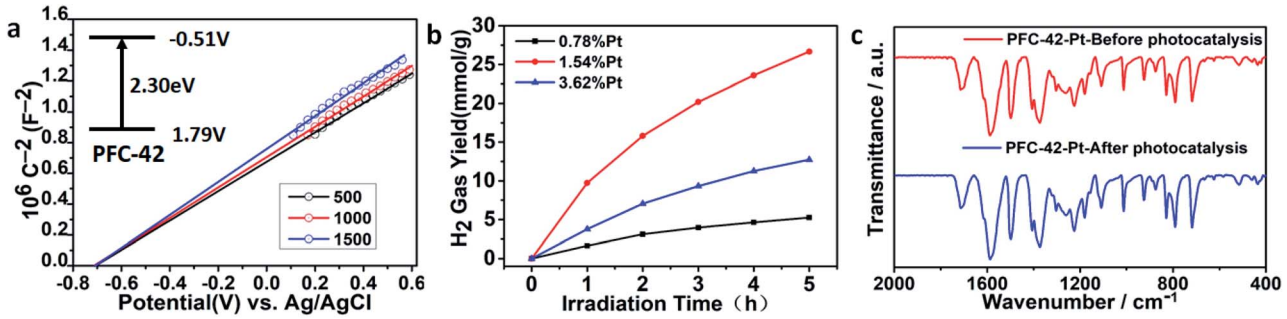

Fig. 2 (a) Mott–Schottky plot of the PFC-42 electrode and the estimated band edge positions of PFC-42 (inset: band structure diagram). (b) The photocatalytic H_2 evolution rate of PFC-42 with different Pt loading amounts. (c) FT-IR spectra of PFC-42 before and after photocatalysis.

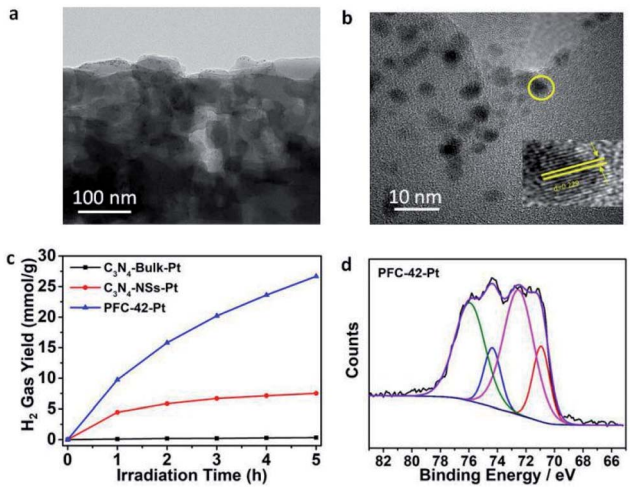

Fig. 3 (a) TEM micrographs of PFC-42 with the uniform distribution of Pt nanoparticles. (b) High-resolution TEM image of 3–5 nm Pt nanoparticles on PFC-42, showing the planes of Pt with the d spacing of 0.229 nm. (c) Photocatalytic H_2 generation activity of bulk C_3N_4–Pt, sheet C_3N_4–Pt, and PFC-42-Pt under the same reaction conditions. (d) High-resolution Pt 4f XPS spectrum.

The influence of the cocatalyst on the photophysical property of PFC-42 was further evaluated by the steady-state photoluminescence (PL) study (Fig. 4a). PFC-42-Pt showed significantly lower PL intensity compared with the pristine PFC-42 and the amorphous ligand, implying that the long-term ordered arrangement of photosensitizers and the incorporation of the Pt cocatalyst can effectively accelerate the photogenerated charge separation and transfer. Moreover, the superposition of two-dimensional PFC-42 layers is expected to induce strong electron coupling between the overlapped hybrid orbitals and form a larger conjugate system, thus facilitating photoinduced carrier transportation,[27,28] which should be another factor contributing to the excellent photocatalytic performance of PFC-42-Pt.

To evaluate the efficient interfacial charge transfer, time-resolved fluorescence decay spectroscopy was performed to provide information about the average lifetime of photo-excited electrons (Fig. 4b). The fluorescence decay curves of the PFC-42-Pt, PFC-42, and ligand are in accordance with two exponential distributions with the average lifetimes of about 80.54 ns, 122.5 ns, and 41.05 ns, respectively. The much longer lifetime of PFC-42 than that of amorphous ligand again indicates that the ordered arrangement of C_3N_4 building units significantly promotes the electron transfer. Pt loading in PFC-42 causes a noticeable decrease in the lifetime, suggesting the possible electron transfer between PFC-42 and Pt. Moreover, photoelectrochemical (PEC) measurements, including photocurrent response (Fig. 4c) and electrochemical impedance spectra (EIS) (Fig. 4d), further implied that PFC-42-Pt enabled effective charge separation during the photocatalysis reaction.

Based on the above discussion, the possible mechanism of PFC-42 for water reduction is illustrated and shown in Fig. 5. First, It should be pointed out that the Pt loaded on the surface of PFC-42 is not active for water reduction under light irradiation; however, it can act as a cocatalyst to accelerate the charge separation of the PFC-42 photocatalyst and the surface catalysis reaction kinetics.[29] Under light irradiation, photogenerated carriers are separated by the strong electron coupling of two-

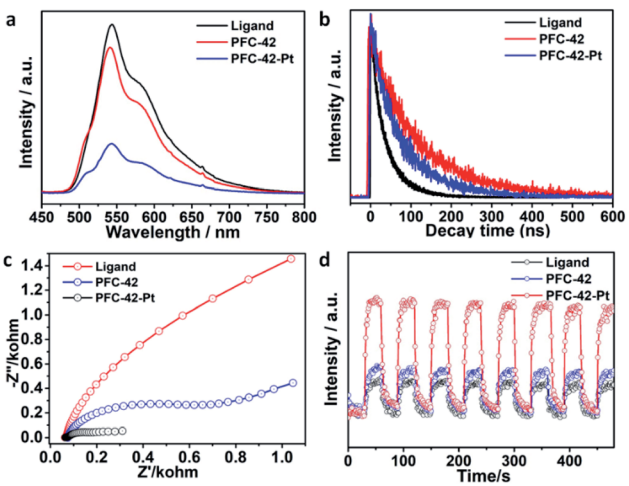

Fig. 4 (a) Room temperature steady-state photoluminescence (PL) spectra under 420 nm excitation for the ligand, PFC-42, and PFC-42-Pt. (b) PL decay spectra monitored at 563 nm under 375 nm excitation for the ligand, PFC-42, and PFC-42-Pt. (c) Electrochemical impedance spectra of the ligand, PFC-42, and PFC-42-Pt. (d) Transient photocurrent response for the ligand, PFC-42, and PFC-42-Pt.

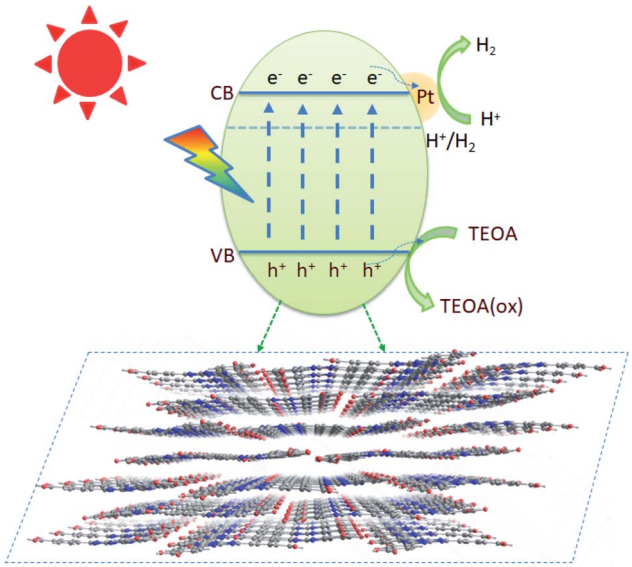

Fig. 5 The proposed mechanism for visible-light-driven photocatalytic H_2 production with PFC-42.

dimensional PFC-42 between the overlapped hybrid orbitals and transferred to the surface of the photocatalyst through a crystallized delocalized system.[30] Then, photogenerated electrons can be transferred to PtNP due to Pt loading in PFC-42 causing a noticeable decrease in the lifetime, highest photocurrent response, and lowest electrochemical impedance spectra. The deposited Pt will be used as the active site for hydrogen production; moreover, the hole is consumed by TEOA, leading to the restraining of the recombination.

Conclusions

In summary, for the first time, a novel heptazine-based HOF PFC-42 has been successfully constructed and carefully characterized. With loading PtNP as the cocatalyst, the obtained material PFC-42-Pt shows excellent photocatalytic hydrogen evolution activity (11.32 mmol g^{-1}). The significantly high H_2 evolution of PFC-42-Pt compared with that of amorphous analogue bulk C_3N_4–Pt and nanosheet C_3N_4–Pt along with recrystallization experiment demonstrate that the ordered arrangement of photosensitizers greatly boosts the photocatalytic activity of the material. We believe that this study as the first HOF material for photocatalysis will open a new door for the application of HOFs in the photocatalytic field.

Conflicts of interest

There are no conflicts to declare.

Acknowledgements

Authors gratefully thank for the support from the National Key Research and Development Program of China (2018YFA0208600), National Natural Science Foundation of China (21871267, 21802142, 22071246), and the Strategic Priority Research Program of the Chinese Academy of Sciences (XDB20000000).

Notes and references

1 C. Gao, J. Low, R. Long, T. Kong, J. Zhu and Y. Xiong, *Chem. Rev.*, 2020, **120**, 12175–12216.
2 Y. Qi and F. Zhang, *Joule*, 2020, **4**, 1364–1366.
3 Z. Wang, C. Li and K. Domen, *Chem. Soc. Rev.*, 2019, **48**, 2109–2125.
4 Y.-J. Gao, X.-B. Li, X.-Z. Wang, N.-J. Zhao, Y. Zhao, Y. Wang, Z.-K. Xin, J.-P. Zhang, T. Zhang, C.-H. Tung and L.-Z. Wu, *Matter*, 2020, **3**(2), 571–585.
5 X.-B. Li, C.-H. Tung and L.-Z. Wu, *Nat. Rev. Chem.*, 2018, **2**(8), 160–173.
6 X.-B. Fan, S. Yu, X. Wang, Z.-J. Li, F. Zhan, J.-X. Li, Y.-J. Gao, A.-D. Xia, Y. Tao, X.-B. Li, L.-P. Zhang, C.-H. Tung and L.-Z. Wu, *Adv. Mater.*, 2019, **31**, 1804872.
7 M. G. Schwab, M. Hamburger, X. Feng, J. Shu, H. W. Spiess, X. Wang, M. Antonietti and K. Muellen, *Chem. Commun.*, 2010, **46**, 8932–8934.
8 C. Yang, B. C. Ma, L. Zhang, S. Lin, S. Ghasimi, K. Landfester, K. A. I. Zhang and X. Wang, *Angew. Chem., Int. Ed.*, 2016, **55**, 9202–9206.
9 L. Wang, X. Zheng, L. Chen, Y. Xiong and H. Xu, *Angew. Chem., Int. Ed.*, 2018, **57**, 3454–3458.
10 R. S. Sprick, B. Bonillo, R. Clowes, P. Guiglion, N. J. Brownbill, B. J. Slater, F. Blanc, M. A. Zwijnenburg, D. J. Adams and A. I. Cooper, *Angew. Chem., Int. Ed.*, 2016, **128**, 1824–1828.
11 X. Wang, K. Maeda, A. Thomas, K. Takanabe, G. Xin, J. M. Carlsson, K. Domen and M. Antonietti, *Nat. Mater.*, 2009, **8**, 76–80.
12 V. Coropceanu, J. Cornil, D. A. da Silva Filho, Y. Olivier, R. Silbey and J.-L. Brédas, *Chem. Rev.*, 2007, **107**, 926–952.
13 Y. He, S. Xiang and B. Chen, *J. Am. Chem. Soc.*, 2011, **133**, 14570–14573.
14 Y. L. Li, E. V. Alexandrov, Q. Yin, L. Li, Z.-B. Fang, W. Yuan, D. M. Proserpio and T.-F. Liu, *J. Am. Chem. Soc.*, 2020, **142**, 7218–7224.
15 D. W. Kang, M. Kang, H. Kim, J. H. Choe, D. W. Kim, J. R. Park, W. R. Lee, D. Moon and C. S. Hong, *Angew. Chem., Int. Ed.*, 2019, **58**, 16152–16155.
16 A. Pulido, L. Chen, T. Kaczorowski, D. Holden, M. A. Little, S. Y. Chong, B. J. Slater, D. P. McMahon, B. Bonillo, C. J. Stackhouse, A. Stephenson, C. M. Kane, R. Clowes, T. Hasell, A. I. Cooper and G. M. Day, *Nature*, 2017, **543**, 657–664.
17 I. Hisaki, *J. Inclusion Phenom. Macrocyclic Chem.*, 2020, **96**, 215–231.
18 I. Hisaki, Y. Suzuki, E. Gomez, Q. Ji, N. Tohnai, T. Nakamura and A. Douhal, *J. Am. Chem. Soc.*, 2019, **141**, 2111–2121.
19 B. Wang, R. He, L. H. Xie, Z. J. Lin, X. Zhang, J. Wang, H. Huang, Z. Zhang, K. S. Schanze, J. Zhang, S. Xiang and B. Chen, *J. Am. Chem. Soc.*, 2020, **142**, 12478–12485.

20 W. Liang, F. Carraro, M. B. Solomon, S. G. Bell, H. Amenitsch, C. J. Sumby, N. G. White, P. Falcaro and C. J. Doonan, *J. Am. Chem. Soc.*, 2019, **141**, 14298–14305.
21 Q. Yin, P. Zhao, R. J. Sa, G. C. Chen, J. Lu, T. F. Liu and R. Cao, *Angew. Chem., Int. Ed.*, 2018, **57**, 7691–7696.
22 S. Cai, H. Shi, Z. Zhang, X. Wang, H. Ma, N. Gan, Q. Wu, Z. Cheng, K. Ling, M. Gu, C. Ma, L. Gu, Z. An and W. Huang, *Angew. Chem., Int. Ed.*, 2018, **57**, 4005–4009.
23 B. T. Liu, E. P. Liu, R. J. Sa and T. F. Liu, *Adv. Opt. Mater.*, 2020, **8**, 2000281.
24 G. Zhang, Z. A. Lan, L. Lin, S. Lin and X. Wang, *Chem. Sci.*, 2016, **7**, 3062–3066.
25 S. Bi, C. Yang, W. B. Zhang, J. S. Xu, L. M. Liu, D. Q. Wu, X. C. Wang, Y. Han, Q. F. Liang and F. Zhang, *Nat. Commun.*, 2019, **10**, 10.
26 Q. Zuo, T. Liu, C. Chen, Y. Ji, X. Gong, Y. Mai and Y. Zhou, *Angew. Chem., Int. Ed.*, 2019, **58**, 10198–10203.
27 X. Ding, J. Guo, X. Feng, Y. Honsho, J. Guo, S. Seki, P. Maitarad, A. Saeki, S. Nagase and D. Jiang, *Angew. Chem., Int. Ed.*, 2011, **50**, 1289–1293.
28 T. Banerjee, K. Gottschling, G. Savasci, C. Ochsenfeld and B. V. Lotsch, *ACS Energy Lett.*, 2018, **3**, 400–409.
29 Y. Xiao, Y. Qi, X. Wang, X. Wang, F. Zhang and C. Li, *Adv. Mater.*, 2018, **30**, 1803401.
30 Z. Zhang, Y. Zhu, X. Chen, H. Zhang and J. Wang, *Adv. Mater.*, 2019, **31**, 1806626.